Longitudinal Static Stability of a Tethered Rotorcraft

by

Brendan James Hernandez

A Thesis Presented in Partial Fulfillment
of the Requirements for the Degree
Master of Science

Approved April 2017 by the
Graduate Supervisory Committee:

Valana Wells, Chair
Fredrick Garrett
Anoop S. Grewal

ARIZONA STATE UNIVERSITY

May 2017

ABSTRACT

This thesis discusses the equilibrium conditions and static stability of a rotorcraft kite with a single main tether flying in steady wind conditions. A dynamic model with five degrees of freedom is derived using Lagrangian formulation, which explicitly avoids any constraint force in the equations of motion. The longitudinal static stability of the steady flight under constant wind conditions is analyzed analytically from the equilibrium conditions. The rotorcraft kite orientation and tether angle are correlated through the equation $\Gamma = \delta - \vartheta$, a necessary condition for equilibrium. A rotorcraft kite design with 3kg mass and 1.25m rotor radius is found to be longitudinally statically stable at 25,000ft with $\Gamma > 65^0$ for wind speeds above 19m/s.

To my parents. Thank you for providing me with every opportunity to succeed in life.

TABLE OF CONTENTS

Page

CHAPTER Page

LIST OF TABLES

Table Page

LIST OF FIGURES

Figure Page

Figure Page

NOMENCLATURE

Roman Letters

C_T = Equilibrium thrust coefficient

C_W = Weight coefficient

d = Shortest distance between two adjacent rotors

G = Center of gravity position of the rotorcraft

I_G = Moment of inertia matrix of the rotorcraft

l = Distance from point Q to point G

$\bar{l}$ = Nondimensionalized l using d

L = Tether length

M = Rotorcraft mass

O = Origin in inertial frame

p = Roll rate of the rotorcraft

q = Pitch rate of the rotorcraft

Q = Bridle point position

Q_i = Generalized forces

r = Yaw rate of the rotorcraft

T_α, T_p, T_q = Thrust stability derivatives

U = Gravitational potential

V_G = Velocity of the rotorcraft Center of mass

W_0 = Wind velocity

Greek Letters

α = Angle of attack

δ = Angle between rotorcraft plane and bridle point

φ = Tether angle in the X-Y inertial plane

Φ = Roll angle of the rotorcraft

Γ = Tether angle from the X-Y inertial plane

$\mathcal{L}$ = Lagrangian function

ϑ = Pitch angle of the rotorcraft

ψ = Yaw angle of the rotorcraft

Subscripts/Superscripts

$(\,)_E$ = Earth fixed (inertial) coordinate frame

$(\,)_B$ = Body fixed coordinate frame

$(\,)^*$ = Equilibrium condition

1. INTRODUCTION

Motivation

Most current methods of generating energy from wind involve wind turbines. According to National Wind Watch, typical wind turbines rise just a few hundred feet in the air. In general, wind speeds increase and remain more constant as altitude increases, up to approximately 40,000ft (Conover and Wentsien). Current methods can thus be improved by accessing the wind at higher altitudes. It is impractical to place a wind turbine at high altitude for structural and other reasons, so many researchers are now considering tethered kite or balloon variants. High altitude tethered kites are the inspiration for this research. The concept is reimagined with a rotorcraft at the end of the tether instead of a standard wing kite.

An advantage of the rotorcraft kite is its ability to hover in the event of little to no wind. As a kite, the high altitude tethered rotorcraft could act as a generator through the rotation of its rotors in the wind. Under normal wind conditions, it would remain in the air through autorotation, but it could use some of the generated and stored electrical energy to power its rotors for flight when wind speed becomes too low for autorotation. This will allow the rotorcraft to remain in the air for as long as desired.

A tethered rotorcraft system has more possible applications than wind energy alone. The ability to stay in the air for long periods of time is beneficial for surveillance and cellular or internet broadcasting as well. Working this problem in its entirety requires analysis of stability and control, power generation, environmental effects, and possible interference with aircraft, at the least. This research will only determine the feasibility of a

tethered rotorcraft from a static stability standpoint and determine possible stable configurations.

Kite Terminology

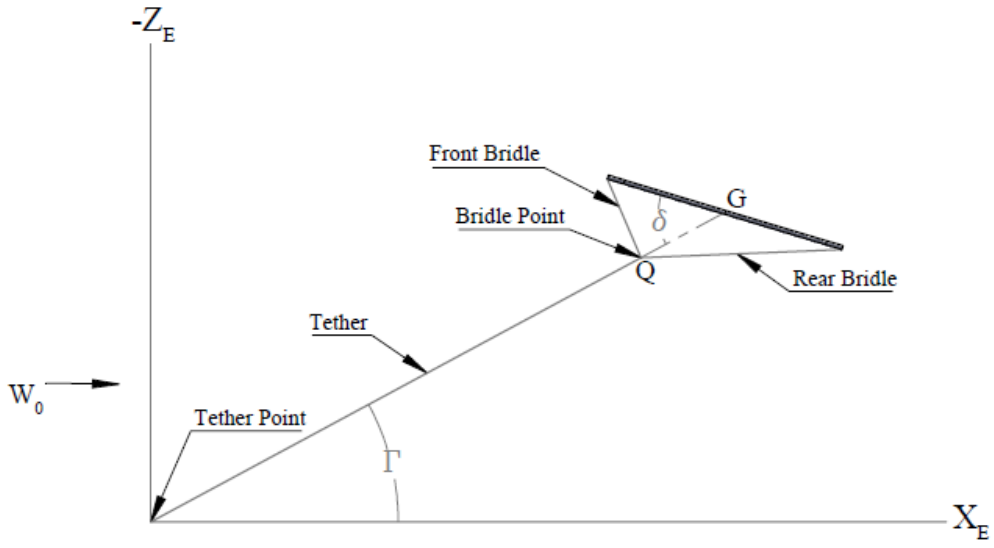

Figure 1. Kite Geometry.

Referring to Fig. 1 above, the tether is defined as the line that runs from the ground to the kite bridle point, Q. The tether angle Γ is the angle between the kite tether and the ground, a larger tether angle corresponds to a higher kite altitude for equivalent tether length. A kite bridle is the combination of lines that attach the kite to the tether at the bridle point. The bridle length is split into the front bridle length and the rear bridle length for most of the models used in this thesis. Varying the front and rear bridle lengths changes the bridle angle δ, which is the angle between the plane of the kite, starting at the kite center of gravity, and the bridle point.

Previous Research

It is important to understand kite and rotor dynamics before analyzing a tethered rotorcraft model. Previous research has been done in both areas and is used to aid in this analysis. Alexander and Stevenson determine the bridle length required for equilibrium of a tethered kite using Newton's Second Law of a static system for the equilibrium condition. They set out to explain how to predict where single or two-line kites will settle during flight. The analysis is performed for a two-dimensional system in the longitudinal plane. The system is defined as a grounded tether connected to front and rear bridle lines, which attach to the front and rear of a flat kite, respectively. Equilibrium points were determined using two constraints, the sum of the external forces on the kite are equal to zero and the sum of the moments about the bridle point are equal to zero. The method laid out in this paper allows for the calculation of the front and rear bridle lengths, and thus angle of the kite relative to the bridle point, required for equilibrium given a certain tether angle, kite weight, and wind velocity. Some of these equilibrium points are unstable which requires further research beyond what Alexander and Stevenson have done to discern from the stable equilibrium points. This research serves as an introduction to the topic of kite mechanics. It uses a simple two-dimensional system and equilibrium analysis that is expanded upon by others in further research.

Sanchez determines the dynamics of a two-dimensional, single line kite using Lagrange's equations. He performs a dynamic analysis on a system equivalent to that used by Alexander and Stevenson in "Kite Equilibrium and Bridle Length". The equations of motion are determined using Lagrange's equations, then the static equilibrium states are found by eliminating time-derivative terms from the equations of motion. The stability of

these equilibrium states is calculated using linear theory and has two eigenmodes; pitch mode and pendulum mode. Next, the dynamic stability of the kite is calculated numerically and stable periodic orbits are found to exist only in a small parametric domain. Finally, he suggests an open loop control system that allows the kite to fly at optimal lift/drag ratios and expresses the limitations of the results. Sanchez's research was an important reference throughout this analysis because Lagrange's equations are used to determine the dynamics of the tethered rotorcraft model.

Losantos and Sanchez-Arriaga discuss the flight dynamics and stability of a kite with a single main line flying in steady and unsteady wind conditions. The equations of motion are determined using Lagrange's equations, then the stability of the steady flight under constant wind conditions is analyzed numerically and analytically. Useful analytical formulas are found for stable-designed kites. Under non-steady wind conditions, the kite stability is explored with the aid of a numerical method based on Floquet theory. The model used in this research is very similar to the model used in this thesis, the difference being the replacement of a kite at the end of the tether with a rotorcraft. The Lagrangian formulation is exactly the same, up to a point, and thus their work is used for comparison and verification purposes during the derivation of the equations of motion of the rotorcraft kite. Also, when further research is conducted on the tethered rotorcraft kite, the dynamic stability results from the steady and unsteady wind conditions will be compared to those presented by Losantos and Sanchez-Arriaga. This will be done in order to compare the dynamics of a kite and a tethered rotorcraft.

Terink, Breukels, Schmehl, and Ockels analyze the flight dynamics and stability of tethered, inflatable airplanes. The system is similar to a tethered kite; one tether attached to the ground, a two-line bridle, and, in this case, an inflatable kiteplane at the end of the bridle lines. Lagrange's equations are used to analyze the dynamics of this system, thus this research provides one more reference for comparison of the Lagrangian analysis done on the tethered rotorcraft kite. Case studies determine that dynamic stability of the inflatable kiteplane requires a small vertical tail plane and a large dihedral angle. The analysis extends to any aircraft-shaped kite, but the kiteplane is used for example calculations and to demonstrate stability trends. This research shows that a lot of thought is being put into new ways of generating sustainable energy. Tethered kites and inflatable objects are being researched thoroughly, and now, rotorcraft kites may be researched more as well.

Williams, Lansdorp, and Ockels study the dynamics and control of a flexible kite. A simple two-plate model with one bridle line on each side and a hinge in the center is used for the analysis. The plates are constrained to have the same yawing angle, but are unconstrained in pitch and roll. Once again, Lagrange's equations are used to obtain the equations of motion. The open-loop system is found to be unstable, causing it to diverge from the equilibrium point with any disturbance unless some kind of active control is used. The controls portion of the research is beyond what is needed for the tethered rotorcraft kite static stability analysis, and is thus not mentioned here. The results show that with controls, a two-plate model can be made stable. It is taken even further with a four-plate model that more accurately describes a flexible kite. The four-plate model is made stable using control as well. The analysis of a 'flexible' kite makes this research unique. It shows

that adding flexibility, which is more realistic for kites, can make the system unstable. This problem was solved, however, using control of the moveable tether points on either side of the kite. Flexibility should not pose problems in future analyses of tethered rotorcraft kites, though, because quadcopters and the like are rigid.

Werle analyzes control volume actuator disk equations for exit velocities equal to or less than zero. He acknowledges that the control-volume actuator-disk model for wind turbines runs into trouble when the downstream velocity at the outlet approaches zero. The work done by Werle provides a new exact solution for induction factors from 0.5 to 1 based on a limit-analysis solution of the control-volume actuator-disk equations. The limit as the domain cross-sectional area approaches infinity is used to obtain the governing equations that provide thrust and power curves as functions of disk loading and velocity induction factor. The relevant result is that for no power, no downstream velocity at the exit of the control-volume, and full blockage, the thrust coefficient of an actuator-disk is two. This is relevant to a tethered rotorcraft kite that will need to autorotate under no power. It is important to determine the thrust produced by a rotor in autorotation and Werle's research aids in that effort.

Georgiou and Theodoropoulos provide an explanation for the deviation between the predictions of the Betz model and the actual results of highly loaded wind turbines. The Betz model approximates the amount of power that can be extracted from free-flowing currents. The research suggests that the one-dimensional flow model used by Betz is too simple. An assumed uniform flow velocity outside of the exit wake profile is replaced with a non-uniform velocity distribution. The distribution deviates further from uniform in

highly loaded cases (when the flow velocity behind the rotor approaches zero). This new control volume is analyzed and new equations are found for the maximum amount of power that can be extracted from free-flowing currents. The results match experimental data well and deviate from the Betz model predictions at higher loading cases. Georgiou and Theodoropoulos conclude that the Betz model is sufficient at low loading, but that it is more accurate to use their method for highly loaded cases. This is applicable to the tethered rotorcraft model due to the expected high loading on the rotors. The analytical and experimental results from their research agree with Werle's research in that the thrust coefficient, for an induction factor of one, is two. This is important for determining the thrust of the rotorcraft during autorotation.

Process

This thesis analyzes the longitudinal static stability of a tethered rotorcraft kite. The rotorcraft has four rotors (quadcopter) with four bridle lines (one attached below each rotor) leading to one tether that attaches at the ground. An empirical extension to an actuator-disk model is used to find an appropriate expression for the thrust of each rotor. The equations of motion are determined using Lagrange's equations. The equilibrium point is calculated from the equations of motion, which leads to two equations that describe the longitudinal static stability of the rotorcraft. A feasible design is determined from the equilibrium equations and the specific conditions under which the design is stable are outlined. The process of determining the equations of motion using Lagrange's equations lays the ground work necessary to analyze the system from a dynamic stability standpoint.

2. DEVELOPMENT

An Earth-fixed inertial coordinate system has origin at the ground tether point, O. The vertical Z_E axis has positive direction downward, and the horizontal wind velocity $\boldsymbol{W}_0$ is assumed to be in the $-X_E$ direction, with Y_E completing the right-hand rule. For convenience, a shorthand will be used for the trigonometric functions sine and cosine. For example, $\sin\alpha$ and $\cos\alpha$ are represented by $s\alpha$ and $c\alpha$.

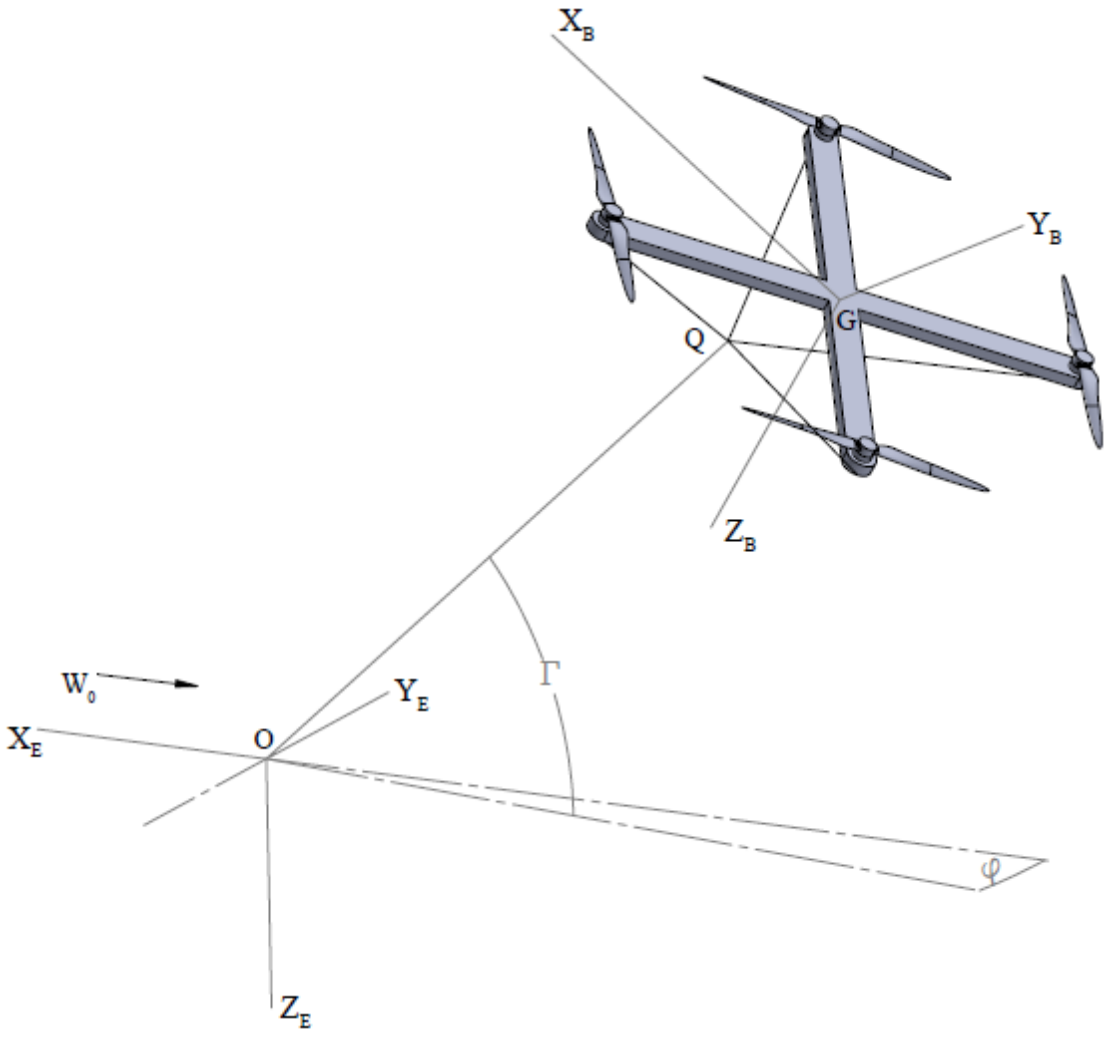

Figure 2. Reference frames and coordinates of the rotorcraft kite model.

The angle Γ represents the inclination of the tether line OQ, and φ is the azimuthal angle of the tether. The position of the bridle point Q, where the tether of length L meets the bridle, is given as

$$\boldsymbol{OQ} = -L(c\Gamma c\varphi \boldsymbol{i}_E + c\Gamma s\varphi \boldsymbol{j}_E + s\Gamma \boldsymbol{k}_E) \tag{1}$$

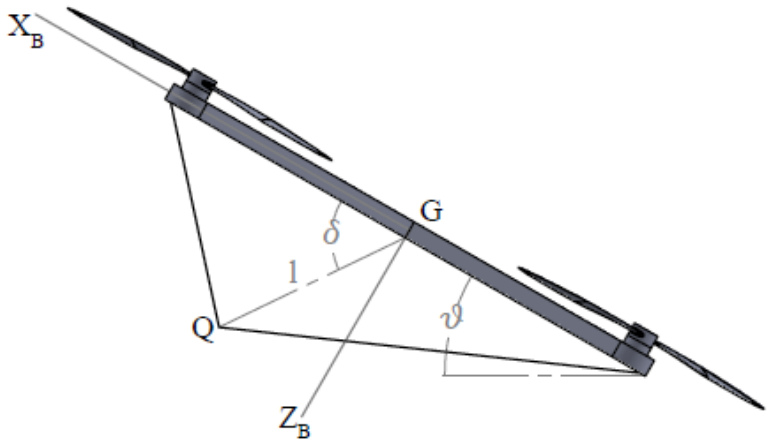

Figure 3. Rotorcraft side view and associated geometry.

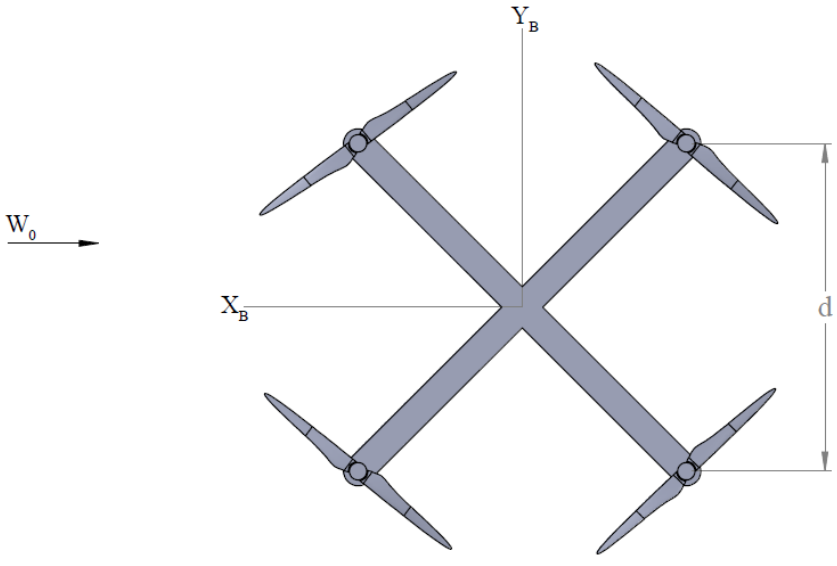

Figure 4. Rotorcraft top view.

The body-fixed coordinate system has origin at the center of mass G of the rotorcraft and axes equal to the principle axes of inertia relative to G, as shown in Fig. 2-4. The inertia matrix in body coordinates is as follows.

$$\boldsymbol{I}_G = \begin{pmatrix} I_x & 0 & 0 \\ 0 & I_y & 0 \\ 0 & 0 & I_z \end{pmatrix} \tag{2}$$

The orientation of the body frame with respect to the inertial frame is determined by Euler angles ϑ, ψ, and ϕ, which correspond to pitch, yaw, and roll angles of the rotorcraft, respectively. The dynamic state vector of the model is then given by

$$\boldsymbol{x} = [\Gamma \ \vartheta \ \varphi \ \psi \ \phi]^T \tag{3}$$

The angular velocity of the rotorcraft in the body frame is given by

$$\boldsymbol{\omega} = (p\boldsymbol{i}_B + q\boldsymbol{j}_B + r\boldsymbol{k}_B) \tag{4}$$

or

$$\boldsymbol{\omega} = \begin{pmatrix} -s\vartheta\dot{\psi} + \dot{\phi} \\ c\phi\dot{\vartheta} + c\vartheta s\phi\dot{\psi} \\ -s\phi\dot{\vartheta} + c\vartheta c\phi\dot{\psi} \end{pmatrix} \tag{5}$$

The rotation matrix **R** is used to convert between inertial and body coordinate frames.

$$\boldsymbol{R} = \begin{pmatrix} c\psi c\vartheta & s\psi c\vartheta & -s\vartheta \\ c\psi s\vartheta s\phi - s\psi c\phi & s\psi s\vartheta s\phi + c\psi c\phi & c\vartheta s\phi \\ c\psi s\vartheta c\phi + s\psi s\phi & s\psi s\vartheta c\phi - c\psi s\phi & c\vartheta c\phi \end{pmatrix} \tag{6}$$

The center of mass position vector is $\boldsymbol{r}_G = \boldsymbol{OQ} + \boldsymbol{QG}$. $\boldsymbol{QG} = -l(c\delta \boldsymbol{i}_B + s\delta \boldsymbol{k}_B)$ where l is the distance from center of mass to bridle point and δ is the angle from the rotorcraft plane to bridle point, as shown in Fig Figure. The rotation matrix is used to convert $\boldsymbol{QG}$ from body frame to inertial frame

$$(\boldsymbol{QG})_{\boldsymbol{E}} = \boldsymbol{R}^{-\mathbf{1}} * (\boldsymbol{QG})_{\boldsymbol{B}} \tag{7}$$

which allows for the calculation of $\boldsymbol{r}_G$

$$\begin{aligned} \boldsymbol{r}_G = &-[Lc\Gamma c\varphi + l(c\psi f_1 + s\delta s\psi s\phi)]\boldsymbol{i}_E \\ &-[Lc\Gamma s\varphi + l(s\psi f_1 - s\delta c\psi s\phi)]\boldsymbol{j}_E \\ &-[Ls\Gamma - lf_2]\boldsymbol{k}_E \end{aligned} \tag{8}$$

where $f_1 = c\delta c\vartheta + s\delta s\vartheta c\phi$ and $f_2 = c\delta s\vartheta - s\delta c\vartheta c\phi$. The velocity vector of the center of mass can be found by taking the time derivative of the position vector.

$$\boldsymbol{V}_G = d\boldsymbol{r}_G/dt \tag{9}$$

The gravitational forces acting on the rotorcraft are considered in the gravitational potential term U where M is the mass of the rotorcraft kite and g is gravity.

$$U(\boldsymbol{x}) = Mg[Ls\Gamma + l(s\delta c\vartheta c\phi - c\delta s\vartheta)] \tag{10}$$

The equations of motion for the rotorcraft were determined using Lagrange's equations.

$$\frac{d}{dt}\left(\frac{d\mathcal{L}}{d\dot{x}_i}\right) - \frac{d\mathcal{L}}{dx_i} = Q_i, \qquad i = 1, \dots, 5 \tag{11}$$

The Lagrangian function, $\mathcal{L}$, is the difference between the kinetic energy and potential energy of the system and Q_i denotes generalized forces that are external to the system or not derivable from a scalar potential function.

$$\mathcal{L} = \frac{1}{2}MV_G^2 + \frac{1}{2}\boldsymbol{\omega} \cdot \boldsymbol{I}_G \cdot \boldsymbol{\omega} - U \tag{12}$$

The equation for generalized force on a rigid body is used. The tether force is not included in the generalized force term because the tether is assumed rigid and the force does no work on the rotorcraft. The remaining force, the thrust of each of the rotors, is summed to provide one resultant force acting at the center of gravity of the rotorcraft and a resulting moment about the same point.

$$Q_i = \left(\sum_{j=1}^{4} \boldsymbol{F}_j^{aero}\right) \cdot \frac{\partial \boldsymbol{V}_G}{\partial \dot{x}_i} + \boldsymbol{M}_G \cdot \frac{\partial \boldsymbol{\omega}}{\partial \dot{x}_i}, \qquad i = 1, \ldots, 5 \tag{13}$$

There is a different aerodynamic force equation for each of the four rotorcraft rotors based on the rotation of the vehicle. The force vector for each rotor is given below.

$$\begin{aligned}
\boldsymbol{F}_1^{aero} &= -\left(T_\alpha \alpha + T_p p - T_q q\right)\boldsymbol{k}_B \\
\boldsymbol{F}_2^{aero} &= -\left(T_\alpha \alpha + T_p p + T_q q\right)\boldsymbol{k}_B \\
\boldsymbol{F}_3^{aero} &= -\left(T_\alpha \alpha - T_p p + T_q q\right)\boldsymbol{k}_B \\
\boldsymbol{F}_4^{aero} &= -\left(T_\alpha \alpha - T_p p - T_q q\right)\boldsymbol{k}_B
\end{aligned} \tag{14}$$

The moment term in Eq. 13 considers the moment about the rotorcraft center of gravity due to the aerodynamic forces. The resultant moment vector is given below.

$$\boldsymbol{M}_G = \left[2T_p d\left(s\vartheta\dot{\psi} - \dot{\phi}\right)\right]\boldsymbol{i}_B - \left[2T_q d\left(c\phi\dot{\vartheta} + s\phi c\vartheta\dot{\psi}\right)\right]\boldsymbol{j}_B \tag{15}$$

T_α, T_p, and T_q are force coefficients, p and q are defined in Eq. 4 and 5, and α is defined in the following equation.

$$\alpha = tan^{-1}\left(\frac{\boldsymbol{V_A}\cdot\boldsymbol{k_B}}{\boldsymbol{V_A}\cdot\boldsymbol{i_B}}\right) \tag{16}$$

More aerodynamic force terms were considered, such as the thrust associated with yawing of the vehicle, $T_r r$, and the thrust associated with the time rate of change of angle of attack, $T_{\dot{\alpha}}\dot{\alpha}$, but were assumed to be small relative to the effects of angle of attack, roll rate, and pitch rate. The intermediate calculations done to obtain $\mathcal{L}$ and Q_i are not shown due to their length and complexity. The final equations of motion, however, are given in Appendix A.

The equilibrium condition is determined by neglecting all time rate of change terms. Doing so results in the equilibrium state $\boldsymbol{x}^*$.

$$\boldsymbol{x}^* = [\Gamma^* \;\; \vartheta^* \;\; 0 \;\; 0 \;\; 0], \qquad \dot{\boldsymbol{x}}^* = 0 \tag{17}$$

The equations that govern the static equilibrium of the rotorcraft are

$$C_W\, c(\delta - \vartheta^*) - 4C_T\, c\delta = 0 \tag{18}$$

$$\Gamma^* = tan^{-1}\left(\frac{4C_T\, c\vartheta^* - C_W}{4C_T\, s\vartheta^*}\right) \tag{19}$$

where the thrust and weight coefficients of the rotorcraft are defined as

$$C_T = \frac{T_\alpha \vartheta}{\frac{1}{2}\rho {V_A}^2 A} = \frac{T}{\frac{1}{2}\rho {V_A}^2 A} \tag{20}$$

and

$$C_W = \frac{Mg}{\frac{1}{2}\rho {V_A}^2 A} \tag{21}$$

Due to the assumption of the wind velocity direction, $T_\alpha \alpha = T_\alpha \vartheta$ in equilibrium. This is the total thrust produced by each of the rotors. There are no thrust contributions from the pitch or roll rate because the vehicle is assumed to be stationary for static equilibrium.

A simple model for the thrust produced by the rotors was created using an extension of disk-actuator theory. The results from Werle agree with Georgiou and Theodoropoulos in that Glauert's empirical data shows that $C_T = 2$ for the zero-power condition. For this analysis, the rotorcraft is in a state of autorotation and no power will be supplied to or extracted from the rotors. As the vehicle angle of attack changes, the wind velocity perpendicular to the rotor plane will also change. The value of C_T determined by Glauert corresponds to that of a rotor with wind velocity entirely perpendicular to the rotor plane. Starting with this value and accounting for the component of velocity perpendicular to the disk results in a simple thrust model given as

$$C_T = 2\ sin\,\alpha^* = 2\ sin\,\vartheta^* \tag{22}$$

Note that when ϑ^* is 90 degrees the wind vector is perpendicular to the rotor plane and the thrust coefficient is two, as measured by Glauert, and when ϑ^* is 0 degrees the wind is parallel with the rotor plane resulting in zero thrust.

The first equilibrium equation, Eq. 18, is nonlinear and requires a numerical determination of the equilibrium pitch angle, ϑ^*. When ϑ^* is calculated, Eq. 19 can be used to analytically determine the equilibrium tether angle, Γ^*.

3. RESULTS

Analysis

Rotorcraft with $\delta = 25^0$

The rotorcraft model is setup such that it has five degrees of freedom, as expressed by the five state variables. The five equations of motion, shown in Appendix A, are the main results of this thesis. Setting the time dependencies to zero results in the equilibrium equations, Eq. 18 and 19. Examination of these equations shows that the only variables that dictate the equilibrium of the model are the thrust and weight coefficients, the tether angle and rotorcraft pitch angle, and the rotorcraft geometry. The following analysis determines relationships among these values that lead to stable equilibrium points. The conditions for stability are more stringent than those for equilibrium, but analyzing equilibrium will help to narrow the options of rotorcraft geometry, weight, and altitude/wind speed that should be tested for stability.

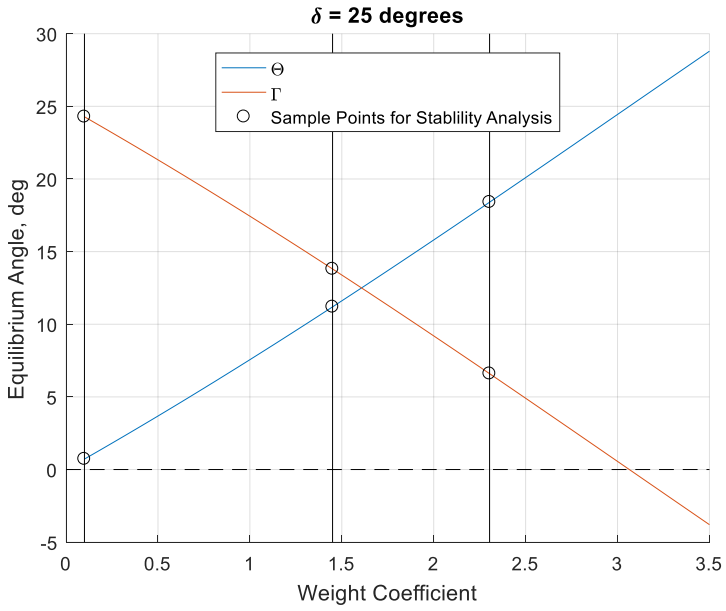

Figure 5. Equilibrium angle vs. weight coefficient.

Fig. 5 shows the tether angle, Γ, and rotorcraft pitch angle, ϑ, required for the system to be in equilibrium at any weight coefficient for a bridle angle $\delta = 25^o$. It is useful to understand the limits of the weight coefficients that provide real equilibrium angles in order to further narrow the combinations of mass, wind velocity, and rotor size that lead to designs capable of equilibrium. At low weight coefficients, the tether angle is large while the pitch angle is small. As the weight coefficient increases, the tether angle decreases until zero while the pitch angle increases. This trend agrees with expectations because as the weight coefficient increases either the wind speed is decreasing, the rotorcraft has a larger mass, or the rotors are smaller. Any of these scenarios would necessitate a higher pitch angle to get a larger component of the wind through the rotors and the tether angle would have to compensate. Fig. 7-9 give a visual representation of this occurring. The minimum weight coefficient corresponds to a tether angle approximately equal to the bridle angle, δ, of the rotorcraft. A horizontal line was added at zero degrees to denote the limit that Γ and ϑ cannot cross. Γ is referenced to the inertial X-Y plane whose origin is located at the ground attachment point of the tether. Thus, if Γ is less than zero degrees, the tether is dipping below Earth's surface. This physically does not make sense and eliminates the possibility of placing the rotorcraft at high altitude. ϑ cannot be less than zero degrees because the wind needs to flow upwards through the rotors for autorotation to occur. If theta is less than zero, the rotorcraft would have a forward tilt similar to a powered rotorcraft in forward flight. However, this rotorcraft is not powered and thus must autorotate with the wind flowing upward through its blades. The three vertical lines

correspond to three sample points which are used to check for static stability and visualize the system with the given bridle angle.

Table 1. Weight coefficients and corresponding equilibrium angles for the rotorcraft geometry with a bridle angle of 25 degrees.

	Sample Point 1	Sample Point 2	Sample Point 3
Weight Coefficient	0.10	1.45	2.30
Gamma, deg	24.28	13.80	6.60
Theta, deg	0.72	11.20	18.40

A small, medium, and large weight coefficient were chosen for the sample points for two reasons. Firstly, for a system such as this, having three statically stable equilibrium points at the low, medium, and high end of the weight coefficient range implies that all the points between them are statically stable. Secondly, it allows for a visual representation that depicts close to the entire possible flight range of the rotorcraft.

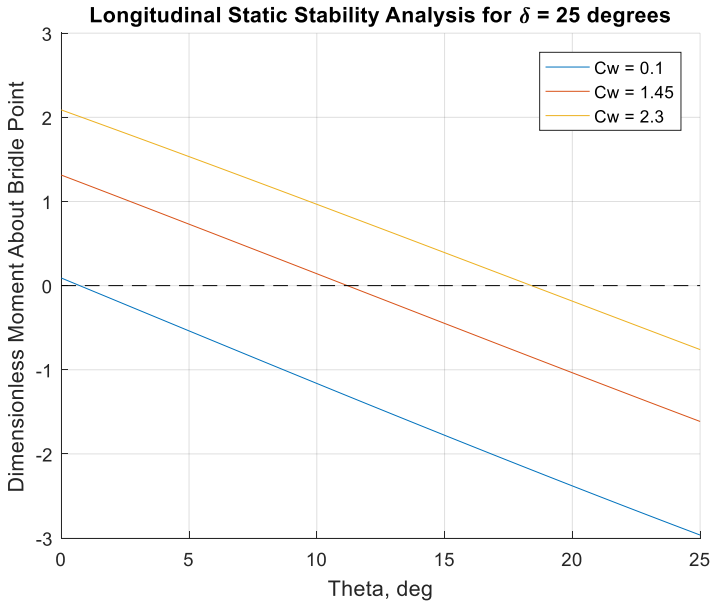

Figure 6. Pitching moment vs. pitch angle.

Fig. 6 is a moment coefficient vs. pitch angle plot that shows the rotorcraft geometry with $\delta = 25^0$ is longitudinally statically stable. The negative slope of all three

lines indicates that they are statically stable, meaning if the rotorcraft is in an equilibrium position and is perturbed, the forces will provide a restoring moment. By looking at any of the curves it can be seen that if the pitch is increased from an equilibrium angle (zero moment), the moment becomes negative which corresponds to a pitch-down moment. The increased pitch is thus countered by the forces providing a pitch-down moment. The same idea applies to a decrease in pitch from an equilibrium angle. If the pitch is decreased, the moment goes positive, producing a pitch-up moment. The decreased pitch creates forces that provide a restoring moment back to the angle that provided zero moment. It is assumed that due to the longitudinal static stability of these three sample points, any weight coefficient in between them has a tether and pitch equilibrium angle that is longitudinally statically stable as well.

The following three figures give a visual representation of the rotorcraft geometry with $\delta = 25^0$ at the three sample points.

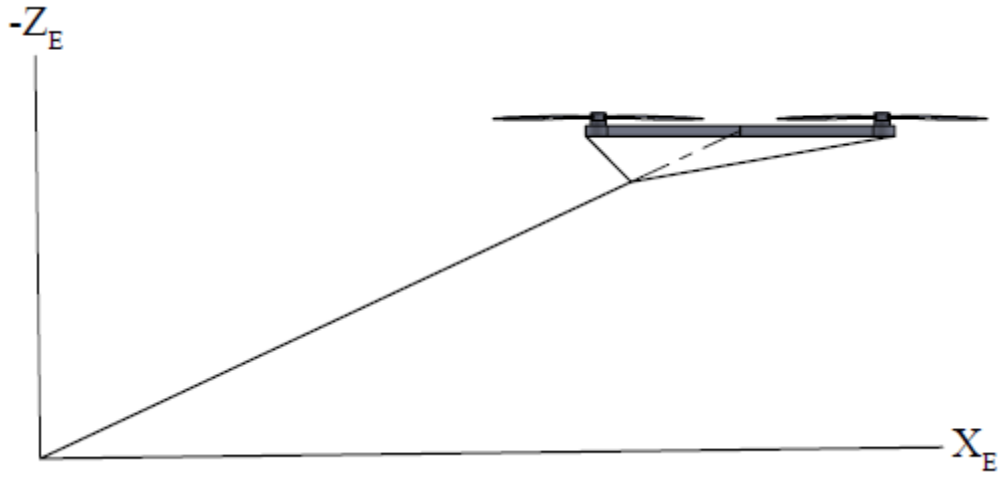

Figure 7. Visualization of rotorcraft equilibrium sample point 1. $\delta = 25^0, \Gamma = 24^0, \vartheta = 0.7^0$.

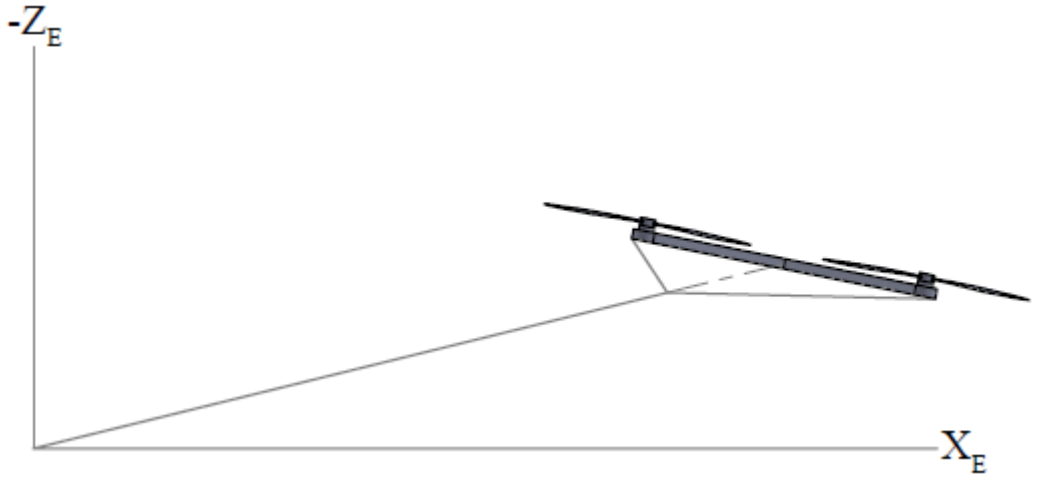

Figure 8. Visualization of rotorcraft equilibrium sample point 2. $\delta = 25^0, \Gamma = 13.8^0, \vartheta = 11.2^0$.

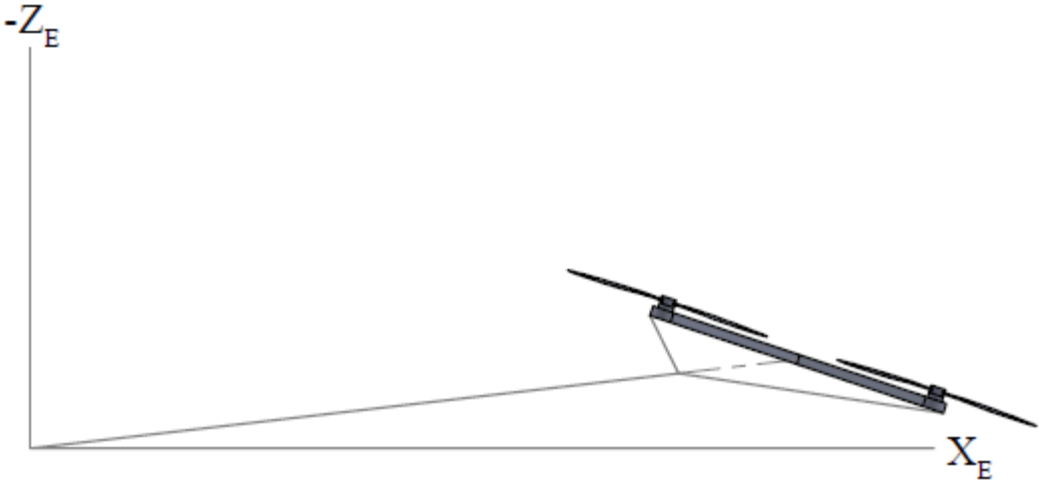

Figure 9. Visualization of rotorcraft equilibrium sample point 3. $\delta = 25^0, \Gamma = 6.6^0, \vartheta = 18.4^0$.

Equilibrium Condition

Fig. 7-9 show that the line that connects the center of mass and the bridle point has the same angle relative to the ground as the tether line for all three samples taken. This relationship is defined by the following equation.

$$\Gamma = \delta - \vartheta \tag{23}$$

Eq. 23 can be derived from the two equilibrium equations, Eq. 18 and 19, and is a requirement for equilibrium. Fig. 10 shows the free body diagram of the tethered rotorcraft kite. The thrust provided by each rotor is equal in equilibrium, and thus the thrust acts at the center of gravity, directly in the center of each of the four rotors. The weight force also acts at the center of gravity; thus, the tether force must also act through the center of gravity for the moments to sum to zero. This requires the line connecting the center of mass and the bridle point to have the same direction as the tether.

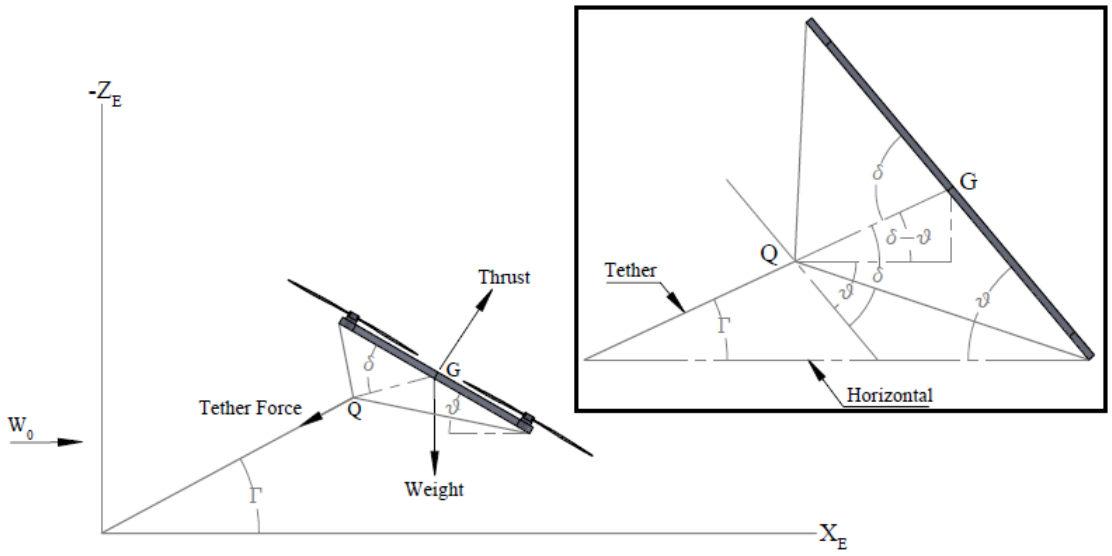

Figure 10. Free body diagram of rotorcraft kite. Subfigure shows relationship between Γ and $\delta - \vartheta$.

Rotorcraft with $\delta = 45^0$

The same analysis was done for a rotorcraft with different geometry, namely a bridle angle of 45 degrees.

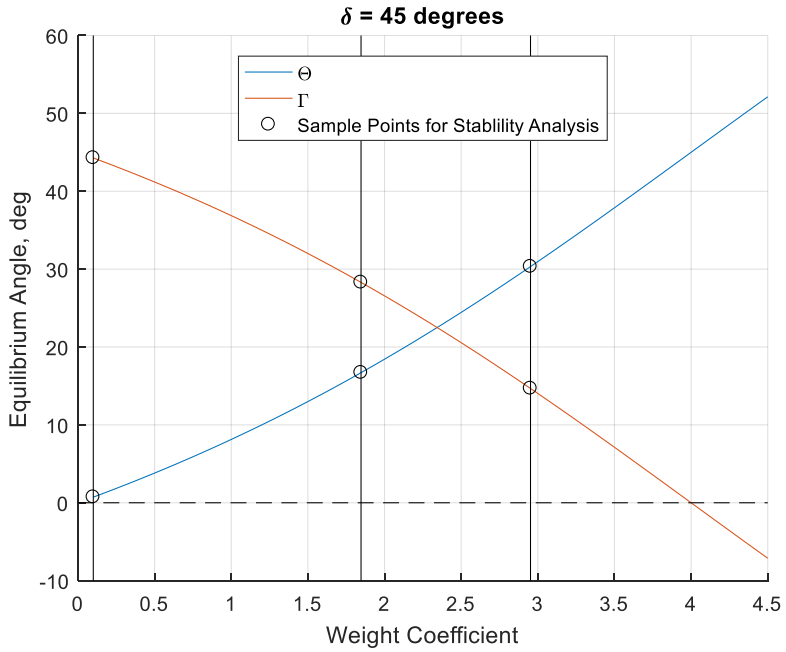

Figure 11. Equilibrium angle vs. weight coefficient.

The trend of the equilibrium angles in Fig. 11 matches that of the $\delta = 25^0$ rotorcraft geometry. At low weight coefficients, the equilibrium tether angle is large while the equilibrium pitch angle is small. As the weight coefficient increases, the pitch angle increases and the tether angle decreases until it reaches zero degrees, at which point the equilibrium angles no longer represent a physically possible state. Another commonality between the equilibrium results of the two different rotorcraft geometries is that the maximum equilibrium tether angle is approximately equal to the bridle angle of the rotorcraft. One major difference between the equilibrium characteristics of the two different rotorcraft designs is that they have different ranges of weight coefficients that

correspond to equilibrium points. The smaller bridle angle geometry has a smaller range of weight coefficients than the larger bridle angle geometry. A larger range of weight coefficients is preferred because it allows for a broader set of system parameters, such as rotorcraft weight and wind velocity, that would lead to an equilibrium condition. Three sample points were taken for this geometry, as well, to test for static stability.

Table 2. Weight coefficients and corresponding equilibrium angles for the rotorcraft geometry with a bridle angle of 45 degrees.

	Sample Point 1	Sample Point 2	Sample Point 3
Weight Coefficient	0.10	1.85	2.95
Gamma, deg	44.27	28.29	14.68
Theta, deg	0.73	16.71	30.32

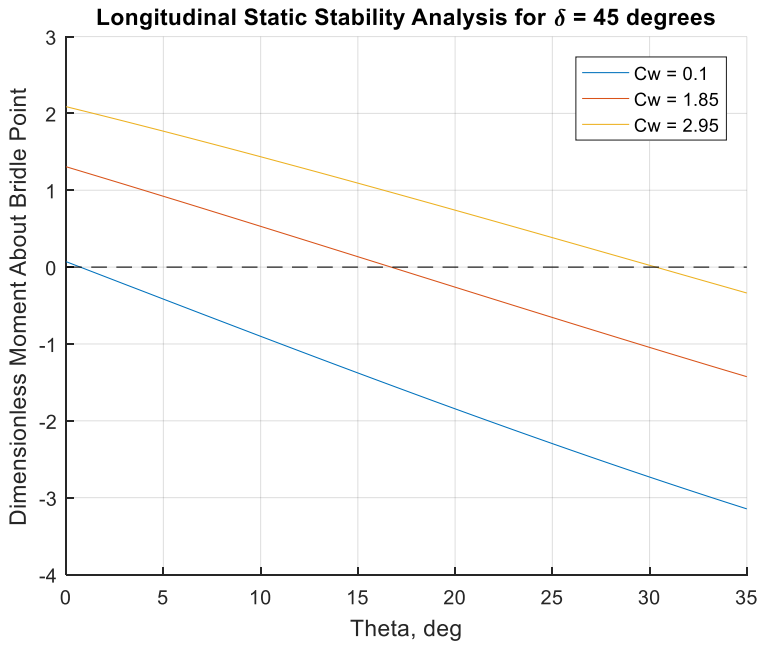

Figure 12. Pitching moment vs. pitch angle.

Fig. 12 shows that the three sample weight coefficients are statically stable in the longitudinal direction. All three samples have negative slopes and thus will have an induced restoring moment if any perturbations from the rotorcraft's equilibrium point are to occur. Once again, it is assumed that all the weight coefficients between these sample points are also longitudinally statically stable. The following three figures give a visual representation of the $\delta = 45^0$ rotorcraft geometry at the three sample points.

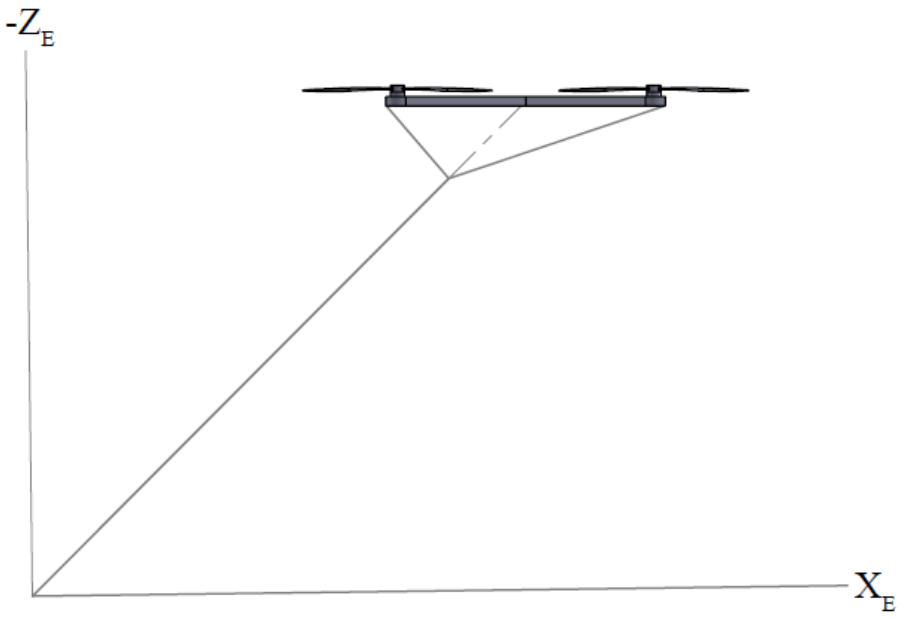

Figure 13. Visualization of rotorcraft equilibrium sample point 1. $\delta = 45^0, \Gamma = 44.3^0, \vartheta = 0.73^0$.

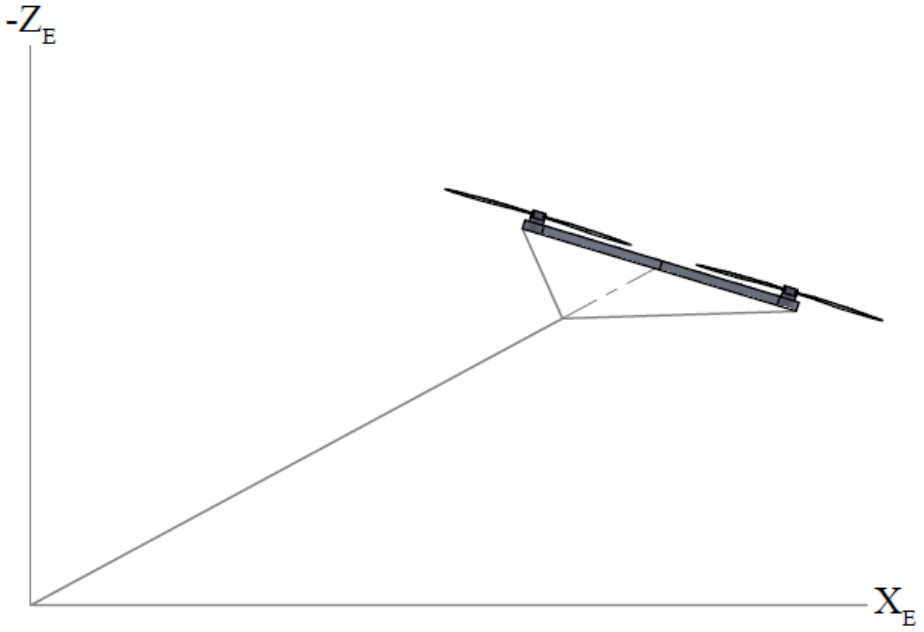

Figure 14. Visualization of rotorcraft equilibrium sample point 2. $\delta = 45^0, \Gamma = 28.3^0, \vartheta = 16.7^0$.

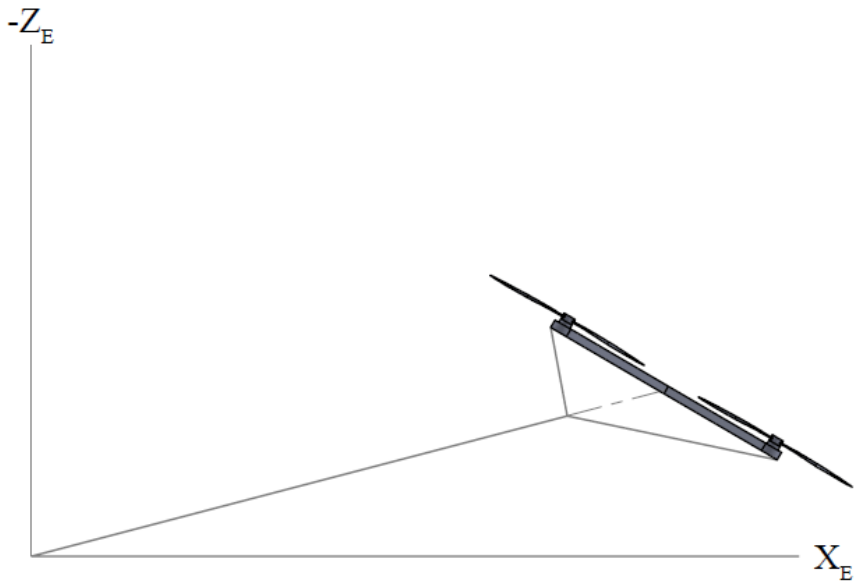

Figure 15. Visualization of rotorcraft equilibrium sample point 3. $\delta = 45^0, \Gamma = 14.7^0, \vartheta = 30.3^0$.

Rotorcraft with $\delta = 80^0$

One final analysis was done for a rotorcraft with a large bridle angle, continuing the trend of testing small, medium, and large bridle angle geometries.

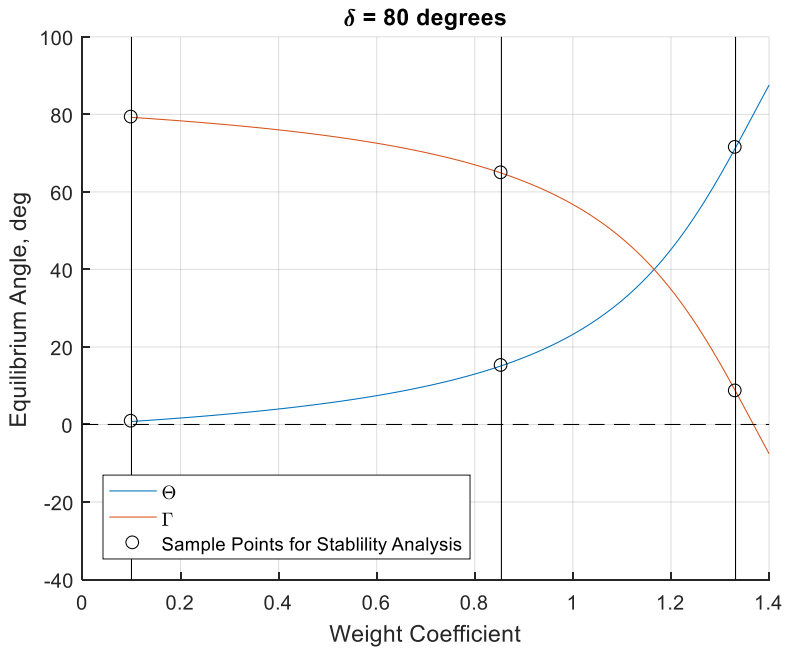

Figure 16. Equilibrium angle vs. weight coefficient.

Fig. 16 shows the same overall equilibrium angle trend as a function of weight coefficient, however, the smaller bridle angle geometries had equilibrium angle curves that were close to linear. For this large bridle angle, the equilibrium angle curves are far from linear. This nonlinear curvature is beneficial for high altitude rotorcraft, though, because there is a larger weight coefficient range that corresponds to large tether angles. Large tether angles make it easier for the rotorcraft to be at a high altitude because it reduces the length of tether needed. Also, the trend from Fig. 5 and Fig. 11 of an increased weight coefficient range with increased bridle angle is not held true for this large bridle angle. The range of weight coefficients that provide positive equilibrium angles for the large bridle

angle geometry is much smaller. This means that initially, increasing bridle angle increases the weight coefficient range, then at some bridle angle the trend reverses and increasing bridle angles reduce the weight coefficient range. The bridle angle at which this trend flips is 45 degrees and corresponds to a maximum weight coefficient range of zero to four. The maximum tether angle is still approximately equal to the bridle angle. Once again, three samples were taken for static stability analysis, as shown in Fig. 17.

Table 3. Weight coefficients and corresponding equilibrium angles for the rotorcraft geometry with a bridle angle of 80 degrees.

	Sample Point 1	Sample Point 2	Sample Point 3
Weight Coefficient	0.10	0.85	1.33
Gamma, deg	79.23	64.85	8.59
Theta, deg	0.77	15.15	71.41

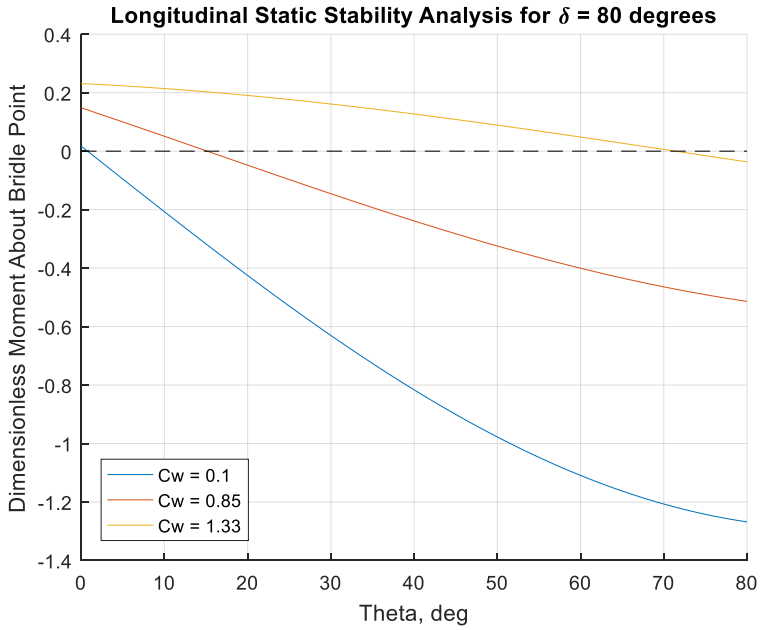

Figure 17. Pitching moment vs. pitch angle.

The figure shows that the three sample points are statically stable in the longitudinal direction. Once again, it is assumed that all weight coefficients between the three samples also have longitudinally statically stable equilibrium angles. An additional assumption based on these results is that all rotorcraft geometries with bridle angles between 25 and 80 degrees have longitudinally statically stable equilibrium points. It is likely that any bridle angle between zero and 90 degrees will provide statically stable equilibrium points, but that assumption requires extrapolation of the three bridle angles tested, rather than interpolation, and is not as reliable. The following three figures give a visual representation of the $\delta = 80^0$ rotorcraft geometry at the three sample points.

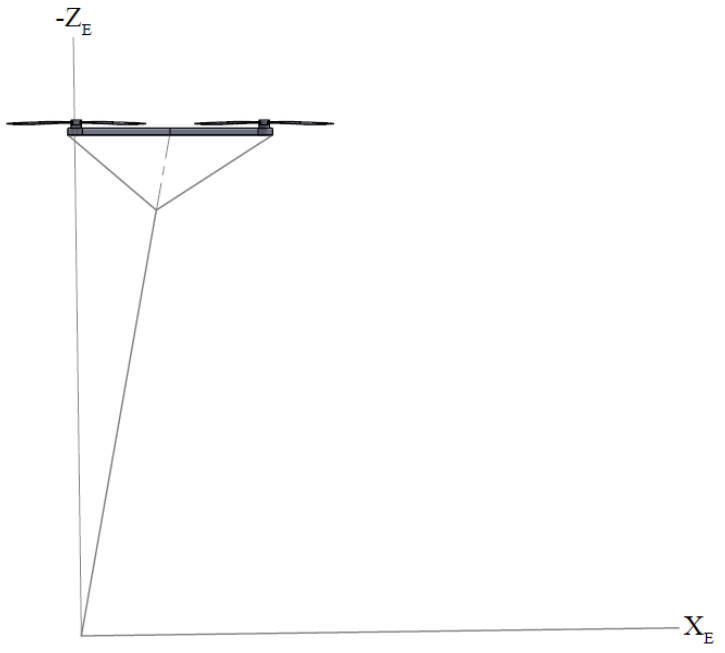

Figure 18. Visualization of rotorcraft equilibrium sample point 1. $\delta = 80^0, \Gamma = 79.2^0, \vartheta = 0.77^0$.

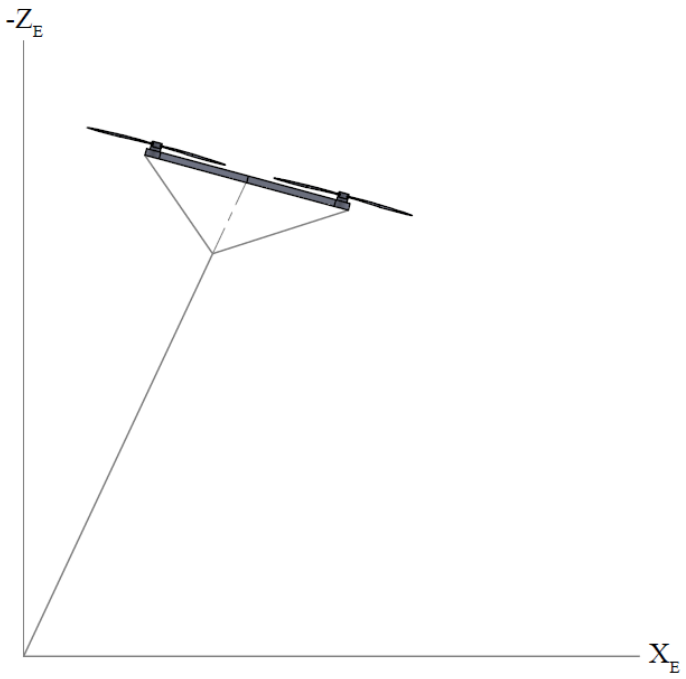

Figure 19. Visualization of rotorcraft equilibrium sample point 2. $\delta = 80^0, \Gamma = 64.9^0, \vartheta = 15.2^0$.

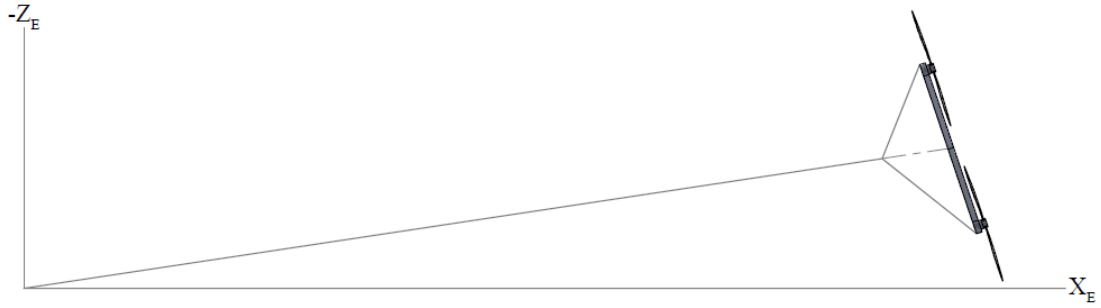

Figure 20. Visualization of rotorcraft equilibrium sample point 3. $\delta = 80^0, \Gamma = 8.59^0, \vartheta = 71.4^0$.

Throughout the equilibrium analysis, the distance from the rotorcraft center of gravity to the bridle point, l, is never varied because it does not appear in the equilibrium equations. Thus, when designing a rotorcraft for this system, the front and rear bridle

lengths can be as long or short as desired, it is only the bridle angle that is important for equilibrium.

The three bridle angles used in Fig. 5, 11, and 16 represent shallow, medium, and large angle geometries, respectively. For the shallow and medium bridle angle cases, equilibrium angles are found for weight coefficients up to three and four, respectively. However, when the bridle angle becomes large, the weight coefficients are more restricted. A larger range of possible weight coefficients is desired due to the flexibility it allows for potential rotorcraft design parameters. At first glance, this implies that large bridle angles should not be used. However, this design is intended for high altitude applications, and real world effects need to be considered. If Γ is a small angle then the tether would need to be extraordinarily long to place the rotorcraft at a high altitude, such as the Jetstream. Also, the horizontal distance needs to be considered because the airspace around this design will most likely be restricted to avoid flying into the rotorcraft or cutting the tether with another aircraft. If the tether is extremely long and travels a large horizontal distance, a very large cylindrical shaped airspace will be restricted. For that reason, a design such as the one used for Fig. 5 should not be considered further due to the low Γ. It should be noted, however, that the model can attain equilibrium in these conditions and might be useful for another design purpose.

At high Γ, the airspace to be restricted would be more like a tall cylinder or tall cylinder slice. The largest Γ equilibrium angle for the medium bridle angle case is approximately 45 degrees, which is still small for the intended applications. The large

bridle angle case, though, can attain Γ equilibrium angles up to 80 degrees, which would be the desired case to place a rotorcraft in the Jetstream.

Rotorcraft with $\delta = 65^0$

The maximum equilibrium tether angle is approximately equal to the bridle angle of a given rotorcraft design. This trend greatly narrows the pool of possible rotorcraft designs to those with large bridle angles. Large bridle angles are desired, but that also restricts the weight coefficients that can be used. A 65-degree tether angle is the minimum angle desired to place a rotorcraft at high altitude. Angles less than this have too large of a horizontal component for practical use. 65 degrees is not a definitive go, no-go, angle, but an approximate minimum desired tether angle chosen for the purpose of presenting the results. A 65-degree minimum tether angle implies that the minimum bridle angle desired is also 65 degrees. Fig. 21 depicts the equilibrium conditions for this minimum bridle angle.

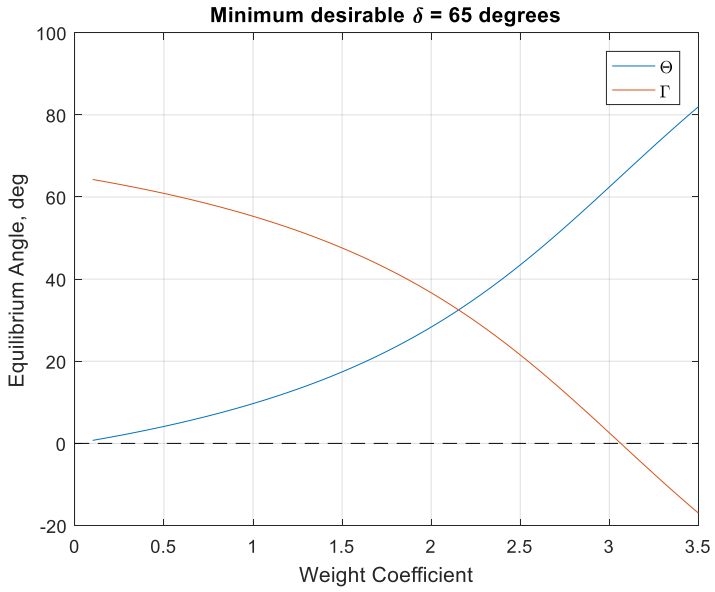

Figure 21. Equilibrium angle vs. weight coefficient.

65 degrees is the minimum desired equilibrium tether angle and the rotorcraft geometry shown above achieves this, but only at a very small weight coefficient. In reality, a larger bridle is required to allow for a range of weight coefficients that provide tether angles larger than 65 degrees. This restricts the possible rotorcraft geometry even further. For example, Fig. 16 shows that a weight coefficient of 0.85 corresponds approximately to a 65-degree tether angle. Any weight coefficient above this will provide an equilibrium tether angle of less than 65 degrees, which would not be ideal. Thus, the 80-degree bridle angle geometry can achieve desired tether angles for any weight coefficient below 0.85. This geometry is close to the ideal geometry. If the bridle angle is increased to 85 degrees, the range of weight coefficients that produce positive tether angles, let alone tether angles above 65 degrees, is greatly reduced. On the other hand, if the bridle angle is decreased to 70 degrees, the range of weight coefficients that produce tether angles above 65 degrees is also reduced.

Design

The minimum and maximum weight coefficients that produce equilibrium tether angles above 65 degrees for the rotorcraft with an 80-degree bridle angle are 0.1 and 0.85, respectively. The minimum weight coefficient value is chosen to be close to, but not equal to, zero. A weight coefficient of zero means nothing and a weight coefficient of 0.1 provides a general lower bound. Fixing the weight coefficient, wind velocity, and altitude allows for the examination of the relationship between the rotorcraft mass and rotor area using Eq. 21.

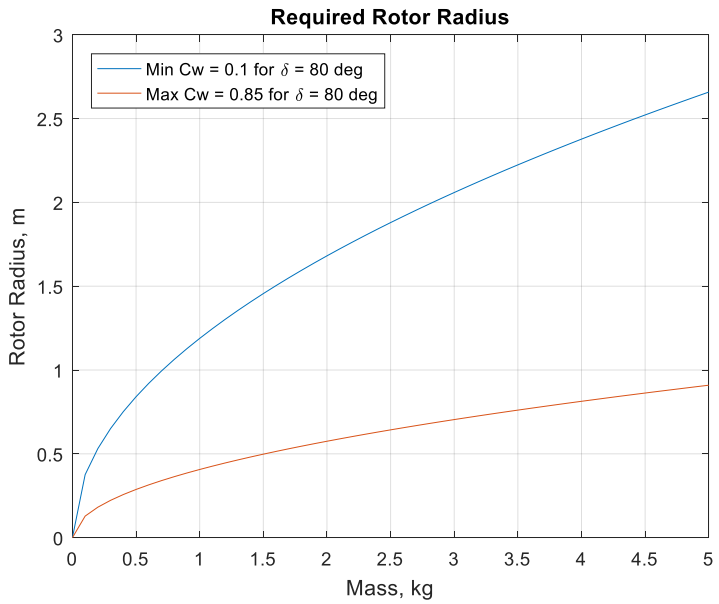

Figure 22. Rotor radius required to achieve desired weight coefficient for a given mass.

Fig. 22 shows the rotor radius required to achieve a desired weight coefficient for any given mass. The assumed altitude is 30,000ft, 5,000ft above the minimum Jetstream altitude, and the assumed wind velocity is 49m/s, which is the average wind speed of the Jetstream. Two curves are shown, corresponding to the minimum and maximum desired weight coefficient for the rotorcraft with an 80-degree bridle angle. If all the weight coefficients between the minimum and maximum were plotted, the curves would fill the space between the two curves in Fig. 22. Thus, any mass and rotor radius combination that fall between the two curves will produce a weight coefficient within the desired range for equilibrium with $\Gamma > 65^0$. Unsurprisingly, Fig. 22 implies that a light rotorcraft with large rotors is desired. This is due to the relatively small weight coefficients that give the desired equilibrium conditions. From this point, a mass and rotor radius combination is selected to

determine the velocity restrictions on such a design. Fig. 23 shows this relationship for a rotorcraft that weighs 3 kg and has a rotor radius of 1.25m.

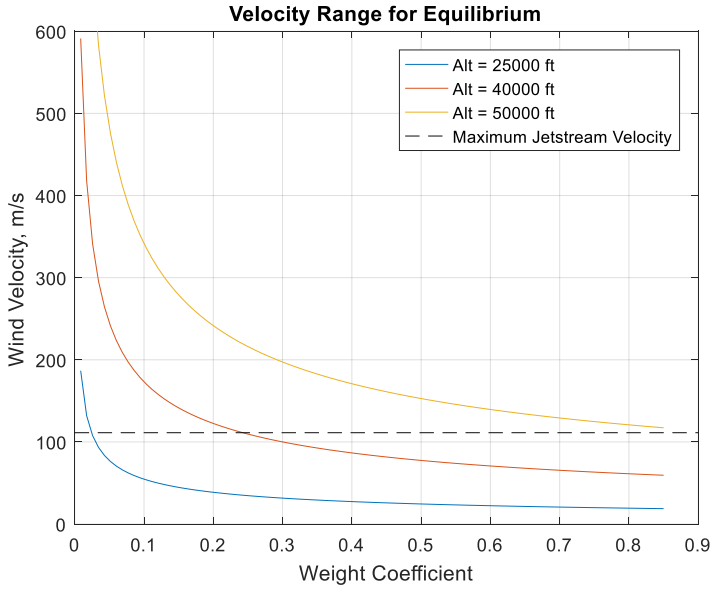

Figure 23. Wind velocity vs. weight coefficient for a rotorcraft design with mass of 3kg and rotor radius of 1.25m.

The three curves correspond to the minimum Jetstream altitude, the maximum Jetstream altitude, and an intermediate altitude. If this particular rotorcraft was placed at 50,000ft the Jetstream would not have fast enough wind for the rotorcraft to attain a low enough weight coefficient for the desired equilibrium conditions. There are regions on the 25,000ft and 40,000ft curves that do fall under the maximum wind speed of the Jetstream, though. This figure shows that the lower Jetstream altitudes are ideal. There is no reason to assume that any region of the Jetstream will consistently have the maximum wind velocity of 112m/s. A low altitude allows for more flexible wind speeds that maintain the desired weight coefficient range. Placing this rotorcraft at 25,000ft would ensure that it maintained a reasonable weight coefficient unless the wind speed dropped below 19m/s.

The purpose of a rotorcraft design instead of a kite, though, is its ability to power its rotors during times of low wind. Thus, if the wind fell below 19m/s the rotorcraft would remain in the air.

The chosen rotorcraft design that weighs 3kg and has a rotor radius of 1.25m can be placed at approximately 25,000ft and will remain longitudinally statically stable with $\Gamma > 65^0$ for wind speeds greater than 19m/s. This is one feasible design based on the equilibrium equations that can later be analyzed for lateral-directional static stability and dynamic stability.

4. CONCLUSION

The equations of motion for a tethered rotorcraft system have been derived. The five degrees of freedom, including two angles, Γ and φ, that describe the state of the tether, and three Euler angles, ϑ, ψ, and ϕ, capture the most important features of the dynamics. Insufficient time has resulted in the lack of a dynamic analysis and will be left for future works. Other considerations for future works are to consider a flexible tether, an effect here ignored, a more in depth analysis of the thrust produced by the rotors, and unsteady wind conditions.

Two equilibrium equations were found that analyzed the system in the X_E-Z_E plane. These equations were used to determine a feasible rotorcraft design. Under steady wind conditions, the equilibrium state of the rotorcraft can be longitudinally statically stable for certain weight coefficients, as shown in Fig. 6, 12, and 17. Relationships were found between the bridle angle of the rotorcraft and the maximum equilibrium tether angle. This relationship helps reduce the range of bridle angles to explore when designing a tethered rotorcraft. It was determined that a high-altitude system should have a large tether angle to reduce the amount of restricted airspace needed. A rotorcraft with an 80-degree bridle angle was chosen for further analysis. The relationship between the rotorcraft mass and rotor area, from Eq. 21, was used to select a possible mass and rotor radius combination. Using this combination, the wind speeds and altitude required for statically stable flight were determined.

Under the current assumptions there are rotorcraft configurations that are longitudinally statically stable at altitudes and wind speeds seen in the Jetstream, although

the system could be stable at lower altitudes and wind speeds as well. One such design with a 3kg mass and 1.25m rotor radius is longitudinally statically stable at 25,000ft with $\Gamma > 65^0$ for wind speeds above 19m/s. This design is still longitudinally statically stable below 19m/s, but would require an equilibrium tether angle less than 65 degrees which was set as the minimum for this design's intended purpose.

REFERENCES

Alexander, K., and J. Stevenson. “Kite equilibrium and bridle length.” *The Aeronautical Journal,* 2001, pp. 535-541.

Conover, W. C., and C. J Wentsien. “WINDS AND TEMPERATURES TO FORTY KILOMETERS.” *Journal of Meteorology,* vol. 12, 1954, pp. 160-164.

Georgiou, D. P., and N. G. Theodoropoulos. “A momentum explanation for the unsatisfactory Betz model prediction in highly loaded wind turbines.” *Wind Energy,* 2011, pp. 653-660.

Losantos, L. Salord, and G. Sanchez-Arriaga. “Flight Dynamics and Stability of Kites in Steady and Unsteady Wind Conditions.” *Journal of Aircraft,* vol. 52, no. 2, 2015, pp. 660-666.

“How big is a wind turbine?” *National Wind Watch,* www.wind-watch.org/faq-size.php. Accessed 19 March 2017.

Sanchez, G. “Dynamics and control of single-line kites.” *The Aeronautical Journal,* 2006, pp. 615-621.

Terink, E. J., et al. “Flight Dynamics and Stability of a Tethered Inflatable Kiteplane.” *Journal of Aircraft,* vol. 48, no. 2, 2011, pp. 503-513.

Werle, M. J. “Passing Through the Wind Turbine Thrust Singularity.” *Journal of Propulsion and Power,* vol. 27, no. 4, 2011, pp. 908-912.

Williams, Paul, et al. “Flexible Tethered Kite with Moveable Attachment Points, Part I: Dynamics and Control.” *AIAA Atmospheric Flight Mechanics Conference and Exhibit, August 2007, Hilton Head, South Carolina,* American Institute of Aeronautics and Astronautics, Inc., 2007.

APPENDIX A

EQUATIONS OF MOTION

The following five equations of motion were determined from Lagrange's equations where $f_1 = c\delta c\vartheta + s\delta s\vartheta c\phi$, $f_2 = c\delta s\vartheta - s\delta c\vartheta c\phi$, $f_3 = s\delta s\vartheta + c\delta c\vartheta c\phi$, and the angle $\nu = \varphi - \psi$.

i = 1 (Γ)

$L^2M\ddot{\Gamma} - LMl(c\Gamma f_1 - s\Gamma f_2 c\nu)\ddot{\vartheta} - LMls\Gamma(s\phi s\delta c\nu + s\nu f_1)\ddot{\psi} + LMls\delta[c\phi s\Gamma s\nu + s\phi(s\Gamma s\vartheta c\nu - c\Gamma c\vartheta)]\ddot{\phi} + LMl(c\Gamma f_2 + s\Gamma c\nu f_1)\dot{\vartheta}^2 + 0.5L^2Mls(2\Gamma)\dot{\phi}^2 + LMls\Gamma(c\nu f_1 - s\phi s\delta s\nu)\dot{\psi}^2 + LMls\delta[s\Gamma(c\phi s\vartheta c\nu - s\phi s\nu) - c\phi c\Gamma c\vartheta]\dot{\phi}^2 + 2LMls\Gamma s\nu f_2\dot{\vartheta}\dot{\psi} + 2LMls\phi s\delta(c\Gamma s\vartheta + s\Gamma c\vartheta c\nu)\dot{\vartheta}\dot{\phi} + 2LMls\delta s\Gamma(s\phi s\vartheta s\nu - c\phi c\nu)\dot{\psi}\dot{\phi} + LMgc\Gamma + 4T_\alpha \tan^{-1}\{[-W(s\phi s\psi + c\phi c\psi s\vartheta) + lc\phi c\delta\dot{\vartheta} + L(s\Gamma(c\phi s\vartheta c\nu - s\phi s\nu) - c\phi c\Gamma c\vartheta)\dot{\Gamma} + ls\phi c\delta c\vartheta\dot{\psi} + Lc\Gamma(s\phi c\nu + c\phi s\vartheta s\nu)\dot{\phi}]/[Wc\psi c\vartheta + lc\phi s\delta\dot{\vartheta} - L(c\Gamma s\vartheta + c\vartheta s\Gamma c\nu)\dot{\Gamma} + ls\phi s\delta c\vartheta\dot{\psi} - Lc\Gamma c\vartheta s\nu\dot{\phi}]\}[Lc\phi c\Gamma c\vartheta - Lc\varphi s\Gamma(s\phi s\psi + c\phi c\psi s\vartheta) + Ls\Gamma s\varphi(s\phi c\psi - c\phi s\psi s\vartheta)]=0$

i = 2 (ϑ)

$LMl(s\Gamma c\nu f_2 - c\Gamma f_1)\ddot{\Gamma} + [c^2\phi I_y + s^2\phi I_z + Ml^2(c^2\phi + c^2\delta - c^2\phi c^2\delta)]\ddot{\vartheta} + LMlc\Gamma s\nu f_2\ddot{\varphi} + s\phi[c\phi c\vartheta(I_y - I_z) - Ml^2s\delta f_2]\ddot{\psi} + Ml^2s\phi c\delta s\delta\ddot{\phi} + LMl(s\Gamma f_1 + c\Gamma c\nu f_2)\dot{\Gamma}^2 + LMlc\Gamma c\nu f_2\dot{\varphi}^2 + [-0.5s(2\vartheta)I_x + (0.5s(2\vartheta) - c\vartheta s\vartheta c^2\phi)I_y + Ml^2c\delta(c\delta c\vartheta s\vartheta(1 + c^2\phi) - c\phi s\delta c(2\vartheta))]\dot{\psi}^2 + Ml^2c\phi c\delta s\delta\dot{\phi}^2 - 2LMls\Gamma s\nu f_2\dot{\Gamma}\dot{\varphi} + [Ml^2(2c\phi s\phi c^2\delta - s(2\phi)) - s(2\phi)(I_z - I_y)]\dot{\vartheta}\dot{\phi} + [c\vartheta I_x + c\vartheta c(2\phi)(I_y - I_z) - 2Ml^2c\phi s\delta f_2]\dot{\psi}\dot{\phi} + 2T_q dc^2\phi\dot{\vartheta} + 2T_q dc\phi s\phi c\vartheta\dot{\psi} - Mglf_1 - 4T_\alpha lc\phi c\delta \tan^{-1}\{[-W(c\phi c\psi s\vartheta + s\phi s\psi) + L(c\phi c\Gamma c\vartheta - s\phi s\Gamma s\nu + c\phi s\Gamma s\vartheta c\nu)\dot{\Gamma} + lc\phi c\delta\dot{\vartheta} + Lc\Gamma(s\phi c\nu - c\phi s\vartheta s\nu)\dot{\varphi} + ls\phi c\delta c\vartheta\dot{\psi}]/[Wc\psi c\vartheta - L(c\Gamma s\vartheta + s\Gamma c\vartheta c\nu)\dot{\Gamma} + lc\phi s\delta\dot{\vartheta} - Lc\Gamma c\vartheta s\nu\dot{\varphi} + ls\phi s\delta c\vartheta\dot{\psi}]\}=0$

i = 3 (φ)

$Mls\nu f_2\ddot{\vartheta} + LMc\Gamma\ddot{\varphi} + Ml(c\nu f_1 - s\phi s\delta s\nu)\ddot{\psi} + Mls\delta(s\phi s\vartheta s\nu - c\phi c\nu)\ddot{\phi} + Mls\nu f_1\dot{\vartheta}^2 + Ml(s\phi s\delta c\nu + s\nu f_1)\dot{\psi}^2 + Mls\delta(s\phi c\nu + c\phi s\vartheta s\nu)\dot{\phi}^2 - 2LMs\Gamma\dot{\Gamma}\dot{\varphi} - 2Mlc\nu f_2\dot{\vartheta}\dot{\psi} + 2Mls\phi s\delta c\vartheta s\nu\dot{\vartheta}\dot{\phi} - 2Mls\delta(c\phi s\nu + s\phi s\vartheta c\nu)\dot{\psi}\dot{\phi} - 4T_\alpha(s\phi c\nu + c\phi s\vartheta s\nu)\tan^{-1}\{[-W(c\phi c\psi s\vartheta + s\phi s\psi) + L(-c\phi c\Gamma c\vartheta - s\phi s\Gamma s\nu + c\phi s\Gamma s\vartheta c\nu)\dot{\Gamma} + lc\phi c\delta\dot{\vartheta} + Lc\Gamma(s\phi c\nu + c\phi s\vartheta s\nu)\dot{\varphi} + ls\phi c\delta c\vartheta\dot{\psi}]/[Wc\psi c\vartheta - L(c\Gamma s\vartheta + c\vartheta s\Gamma c\nu)\dot{\Gamma} + lc\phi s\delta\dot{\vartheta} - Lc\Gamma c\vartheta s\nu\dot{\varphi} + ls\phi s\delta c\vartheta\dot{\psi}]\}=0$

i = 4 (ψ)

$-LMls\Gamma(sv f_1 + s\phi s\delta cv)\ddot{\Gamma} + s\phi\left[Ml^2(c\phi c\vartheta - c\delta f_3) + c\phi c\vartheta\left(I_y - I_z\right)\right]\ddot{\vartheta} +$
$LMlc\Gamma(cv f_1 - s\phi s\delta sv)\ddot{\varphi} + \left[s^2\vartheta I_x + s^2\phi c^2\vartheta I_y + c^2\phi c^2\vartheta I_z + Ml^2\left(s^2\delta -\right.\right.$
$\left.\left.c^2\vartheta c^2\phi s^2\delta + c\phi c\delta s\delta s(2\vartheta)\right)\right]\ddot{\psi} - (s\vartheta I_x - Ml^2 s^2\delta f_3)\ddot{\phi} - LMlc\Gamma(sv f_1 + s\phi s\delta cv)\dot{\Gamma}^2 +$
$s\phi\left[c\phi s\vartheta\left(I_z - I_y\right) - Ml^2 s\delta f_1\right]\dot{\vartheta}^2 - Lmlc\Gamma(sv f_1 + s\phi s\delta cv)\dot{\varphi}^2 + Ml^2 s\phi c\delta s\delta c\vartheta\dot{\phi}^2 +$
$2LMls\Gamma(s\phi s\delta sv - cv f_1)\dot{\Gamma}\dot{\phi} + \left[s(2\vartheta)\left(I_x - s^2\phi I_y - c^2\phi I_z\right) + Ml^2\left(s(2\vartheta)(c^2\phi s^2\delta -\right.\right.$
$\left.\left.c^2\delta) + s(2\delta)c(2\vartheta)\right)\right]\dot{\vartheta}\dot{\psi} + c\vartheta\left[-I_x + c(2\phi)\left(I_y - I_z\right) - 2Ml^2 s^2\phi s^2\delta\right]\dot{\vartheta}\dot{\phi} +$
$2s\phi c\vartheta\left[c\phi c\vartheta\left(I_y - I_z\right) + Ml^2(c\phi c\vartheta - c\delta f_3)\right]\dot{\psi}\dot{\phi} + 2T_q dc\phi s\phi c\vartheta\dot{\vartheta} + 2d\left(T_q s^2\phi c^2\phi +\right.$
$\left.T_p s^2\vartheta\right)\dot{\psi} - 2T_p ds\vartheta\dot{\phi} - 4s\phi c\delta c\vartheta T_\alpha l\tan^{-1}\{\left[-W(c\phi c\psi s\vartheta + s\phi s\psi) + L(-c\phi c\Gamma c\vartheta -\right.$
$s\phi c\Gamma sv + c\phi s\Gamma s\vartheta cv)\dot{\Gamma} + lc\phi c\delta\dot{\vartheta} + Lc\Gamma(s\phi cv + c\phi s\vartheta sv)\dot{\varphi} + ls\phi c\delta c\vartheta\dot{\psi}\left]/\right[Wc\psi c\vartheta -$
$\left.L(c\Gamma s\vartheta + c\vartheta s\Gamma cv)\dot{\Gamma} + lc\phi s\delta\dot{\vartheta} - Lc\Gamma c\vartheta sv\dot{\varphi} + ls\phi s\delta c\vartheta\dot{\psi}\right]\}$=0

i = 5 (ϕ)

$LMls\delta(c\phi s\Gamma sv - s\phi c\Gamma c\vartheta + s\phi s\Gamma s\vartheta cv)\ddot{\Gamma} + Ml^2 s\phi c\delta s\delta\ddot{\vartheta} + LMlc\Gamma s\delta(s\phi s\vartheta sv -$
$c\phi cv)\ddot{\varphi} - [s\vartheta I_x + Ml^2 s\delta(s\delta + c\phi c\vartheta c\delta)]\ddot{\psi} + (I_x + Ml^2 s^2\delta)\ddot{\phi} + LMls\delta(s\phi c\vartheta s\Gamma +$
$c\Gamma c\phi sv + s\phi c\Gamma s\vartheta cv)\dot{\Gamma}^2 + 0.5s(2\phi)\left(Ml^2 s^2\delta + I_y - I_z\right)\dot{\vartheta}^2 + LMlc\Gamma s\delta(c\phi sv +$
$s\phi s\vartheta cv)\dot{\varphi}^2 + \left[0.5s(2\phi)c^2\vartheta\left(I_z - I_y\right) + Ml^2 s\phi c\vartheta s\delta f_2\right]\dot{\psi}^2 + 2LMls\delta s\Gamma(c\phi cv -$
$s\phi s\vartheta sv)\dot{\Gamma}\dot{\varphi} + \left[-c\vartheta I_x + c\vartheta c(2\phi)\left(I_z - I_y\right) + 2Ml^2 c\phi s\delta f_2\right]\dot{\vartheta}\dot{\psi} - 2T_p ds\vartheta\dot{\psi} + 2T_p d\dot{\phi} -$
$Mgls\phi s\delta c\vartheta$=0